Supporting Information

Synthesis, Magnetism and Mössbauer Studies of Tetranuclear Heterometallic $\{Fe^{III}_2Ln_2\}$(Ln = Gd, Dy, Tb) Complexes: Evidence of Slow Relaxation of Magnetization in the Terbium Analogue

Prasenjit Bag,[a] Joydeb Goura,[a] Valeriu Mereacre,[b] Ghenadie Novitchi,[c] Annie. K. Powell,[b] Vadapalli Chandrasekhar,*[a,d]*

[a]Department of Chemistry, Indian Institute of Technology Kanpur, Kanpur-208016, India;

[b]Institute of Inorganic Chemistry, Karlsruhe Institute of Technology, Engesserstrasse 15, 76128 Karlsruhe, Germany.

[c]Laboratoire National des Champs Magnétiques Intenses, CNRS UPR 3228, 25 Rue des Martyrs, Grenoble, France

[d]National Institute of Science Education and Research, Institute of Physics Campus, Sachivalaya Marg, Sainik School Road, Bhubaneshwar-751 005, Odisha, India

AUTHORS EMAIL ADDRESS: vc@iitk.ac.in; valeriu.mereacre@kit.edu

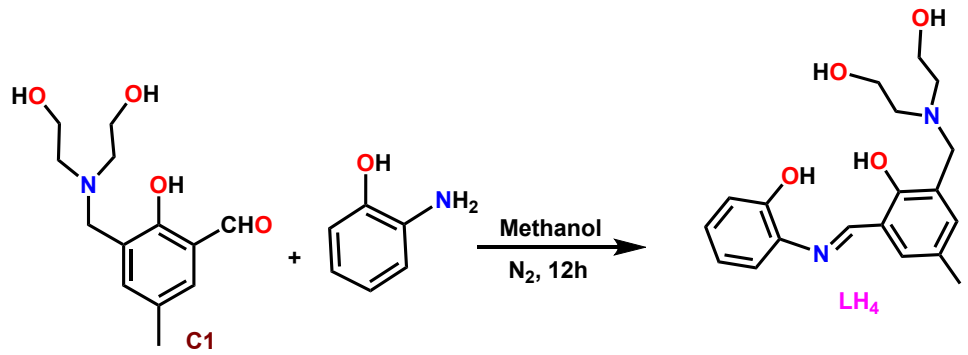

Scheme S1. Synthesis of ligand $\mathbf{LH_4}$

Table S1. Bond valence sum (BVS) calculation for determination of protonation level on oxygen atoms in **1**

Atoms	BVS value
O7	2.052
O8	1.231

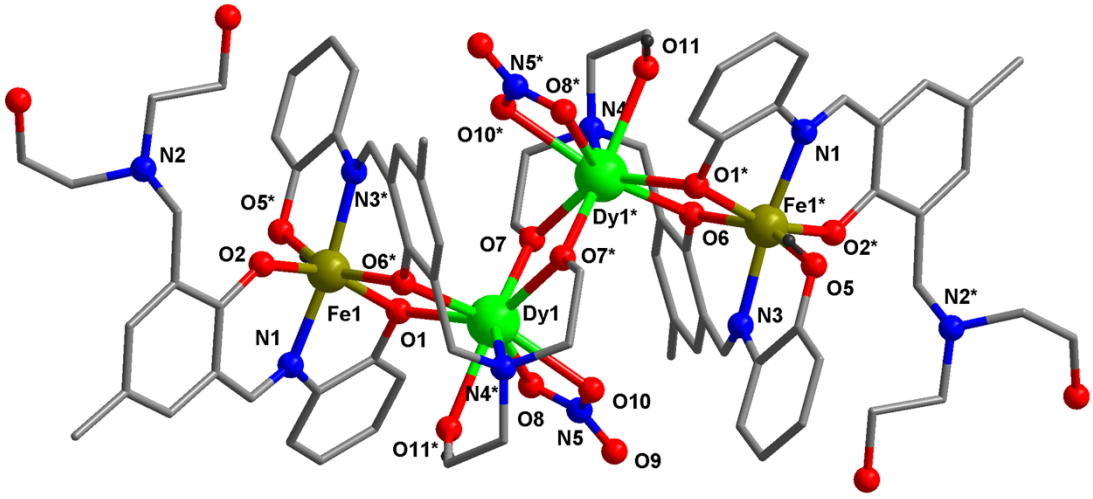

Figure S1. Molecular structure of **2** (Hydrogen atoms, solvent molecules, counter anions and disordered carbon and oxygen atoms were omitted for clarity).

Table S2. Selected bond distances and bond angles for compound **2**

Bond lengths (Å)				Bond angles (°)	
Bond Lengths around Iron(1)		Bond Lengths around Dysprosium(1)			
Fe(1)-O(2)	1.933(3)	Dy(1)-O(7)	2.240(3)	Fe(1)-O(6)-Dy(1)	108.22(13)
Fe(1)-O(5)	1.980(4)	Dy(1)-O(7)*	2.267(3)	Fe(1)-O(1)-Dy(1)	105.84(12)
Fe(1)-O(6)	2.016(3)	Dy(1)-O(6)	2.328(3)	Dy(1)-O(7)-Dy(1)*	110.60(12)
Fe(1)-O(1)	2.048(3)	Dy(1)-O(1)	2.363(3)	Fe(1)-Dy(1)- Dy(1)*	109.43(2)
Fe(1)-N(1)	2.103(4)	Dy(1)-O(11)	2.388(3)		
Fe(1)-N(3)	2.105(4)	Dy(1)-O(10)	2.446(3)		
Fe(1)-Dy(1)	3.5241(13)	Dy(1)-O(8)	2.467(3)		
		Dy(1)-N(4)*	2.591(4)		
		Dy(1)-N(5)	2.864(4)		
		Dy(1)-Dy(1)*	3.7056(10)		

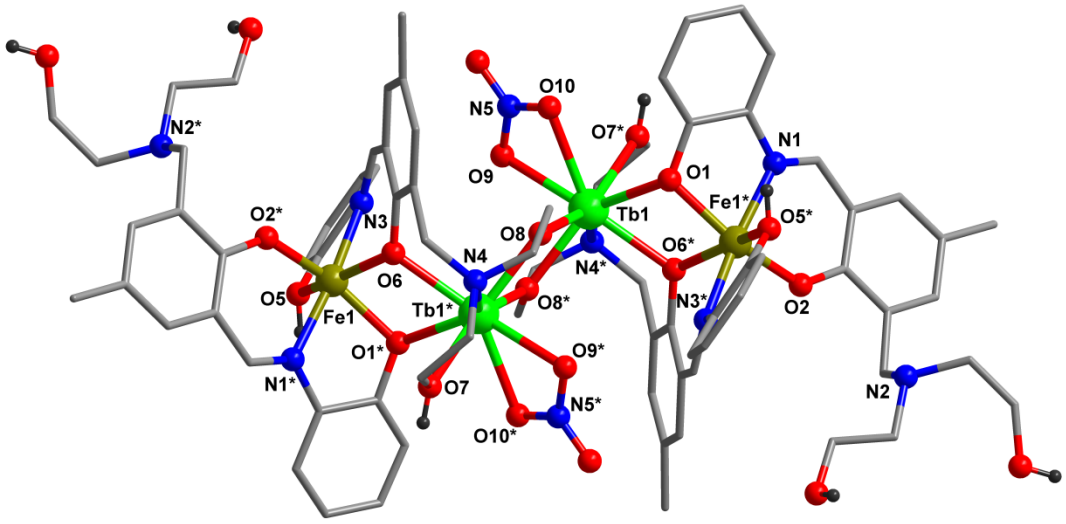

Figure S2. Molecular structure of **3** (Hydrogen atoms, solvent molecules, counter anions and disordered oxygen atoms were omitted for clarity).

Table S3. Selected bond distances and bond angles for compound **3**

Bond lengths (Å)				Bond angles (°)	
Bond Lengths around Iron(1)		Bond Lengths around Terbium(1)			
Fe(1)-O(2)*	1.928(6)	Tb(1)-O(8)	2.264(5)	Tb(1)-O(8)-Tb(1)*	110.8(2)
Fe(1)-O(5)	1.987(6)	Tb(1)-O(8)*	2.266(5)	Fe(1)-O(6)-Tb(1)*	108.0(2)
Fe(1)-O(6)	2.019(5)	Tb(1)-O(6)*	2.339(5)	Fe(1)* -O(1) -Tb(1)	105.7(2)
Fe(1)-O(1)*	2.045(5)	Tb(1)-O(1)	2.380(5)	O(2)*-Fe(1)-O(6)	94.4(2)
Fe(1)-N(3)	2.114(7)	Tb(1)-O(7)*	2.407(6)	O(5) -Fe(1)-O(1)*	92.4(2)
Fe(1)-N(1)*	2.106(7)	Tb(1)-O(9)	2.453(6)	Fe(1)-Dy(1)- Dy(1)*	109.97(4)
Fe(1)-Tb(1)*	3.533(2)	Tb(1)-O(10)	2.504(5)		
		Tb(1)-N(4)*	2.601(6)		
		Tb(1)-Tb(1)*	3.7287(12)		

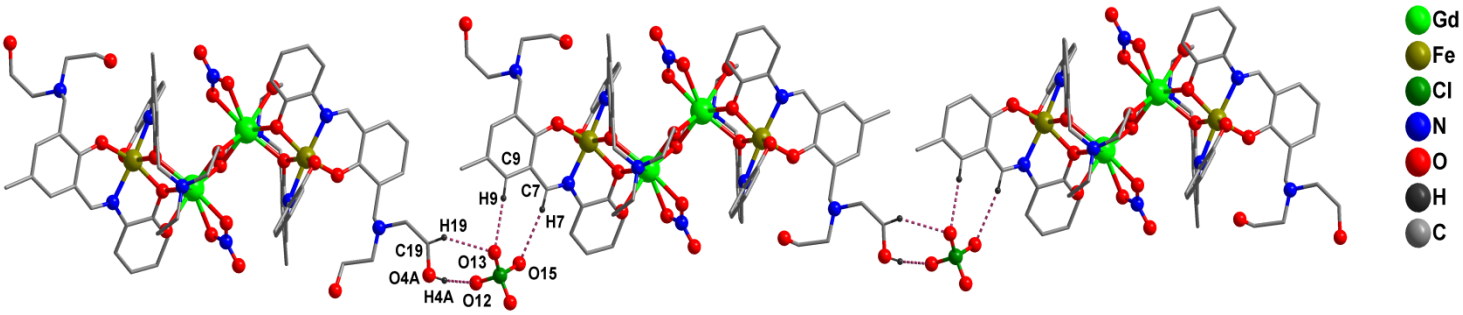

Figure S3: Formation of one dimensional chain through C–H….O interactions in **1** mediated by perchlorate counter anion.

Table S4: Hydrogen bond parameters for compound **1**

Compounds	D–H….A	d(D–H)	d(H….A)	d(D….A)	<(DHA)	Symmetry of A
1	C7–H7….O15	0.930(11)	2.617(16)	3.564(20)	165.094(77)	1-x, 1-y, 1-z
	C9– H9….O13	0.930(12)	2.515(15)	3.435(19)	169.94(78)	1-x, 1-y, 1-z
	C19– H19….O12	0.980(15)	2.636(22)	3.402(30)	135.26 (10)	1-x, 1-y, 1-z
	O3B– H4A….O12	0.819(2)	1.974(16)	2.698(26)	146.96(14)	1-x, 1-y, 2-z

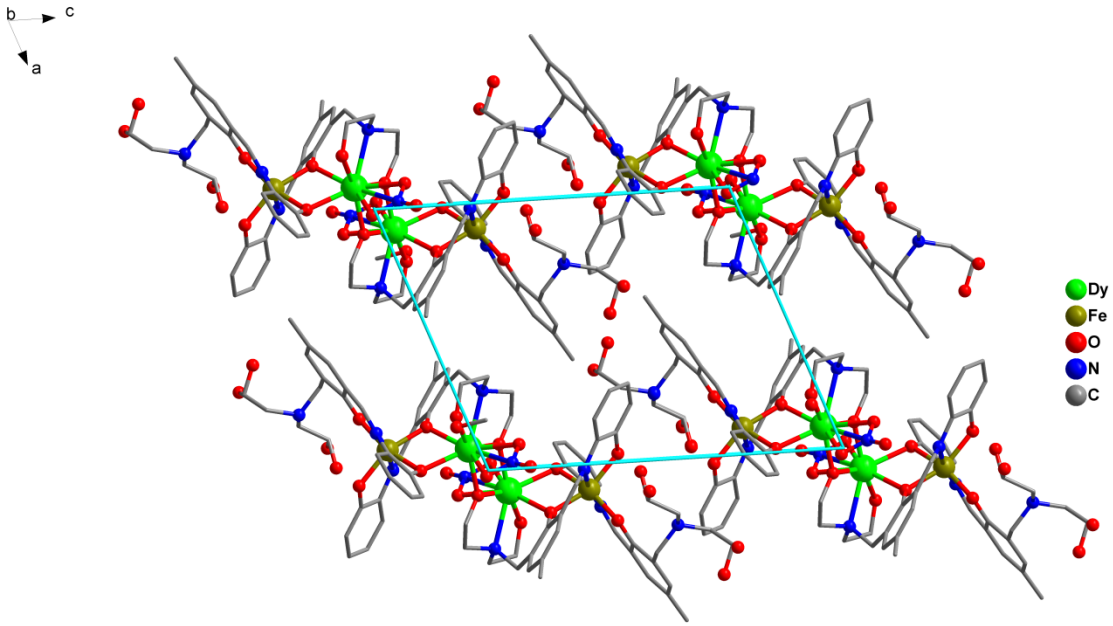

Figure S4: Packing diagram of **2** along Crystallographic ‘b’ axis.

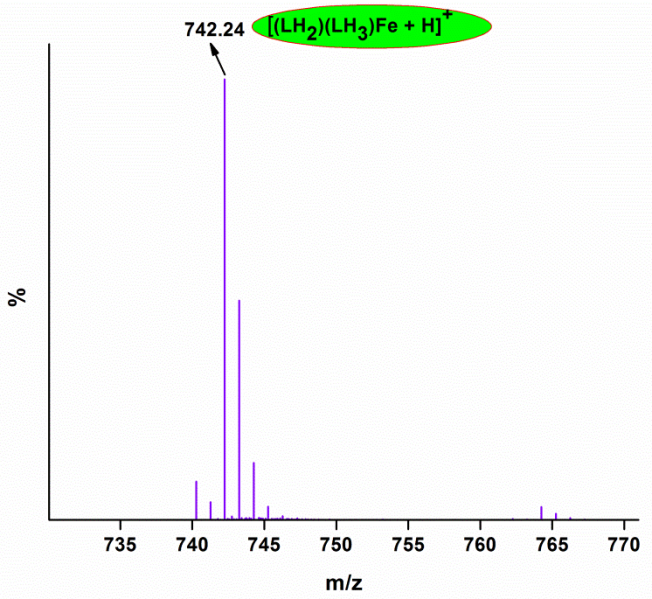

Figure S5. ESI-MS of all three compounds showing the isotopic distribution pattern of common fragment.

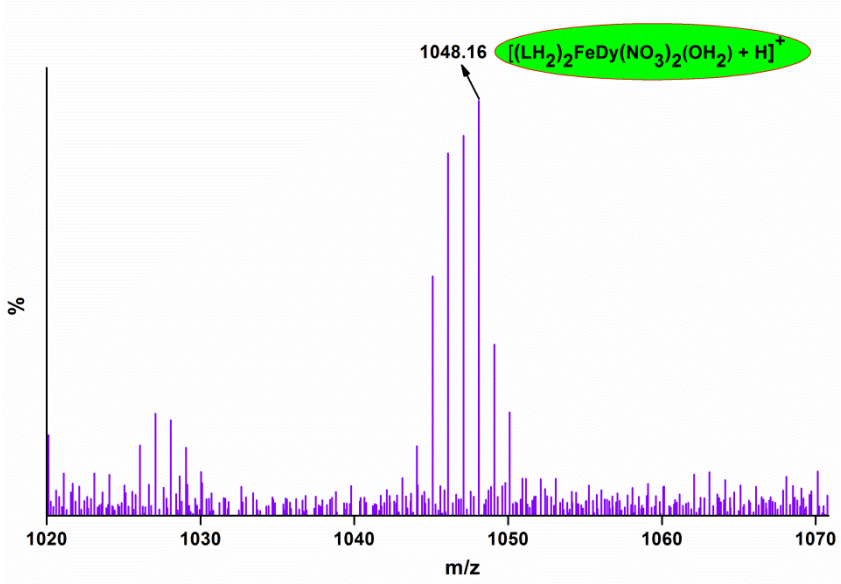

Figure S6. ESI-MS of **2** (shows isotropic distribution pattern of one fragment)

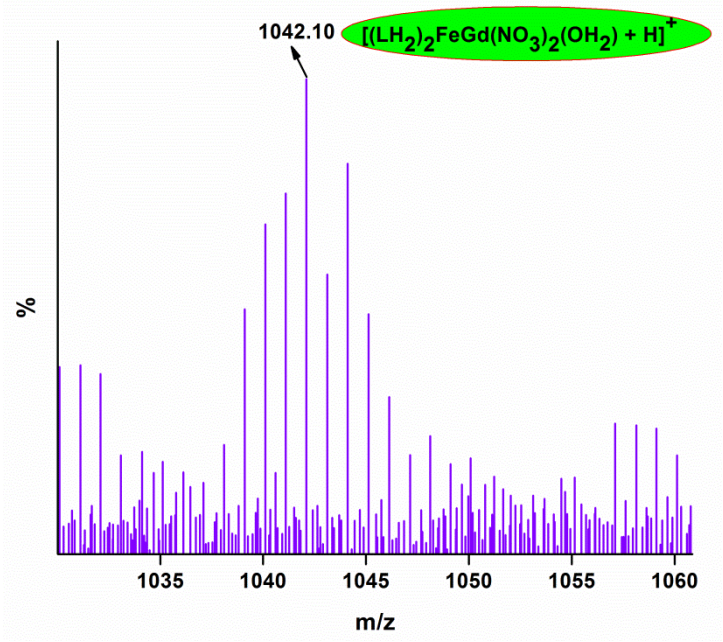

Figure S7. ESI-MS of **1** (shows isotropic distribution pattern of one fragment)

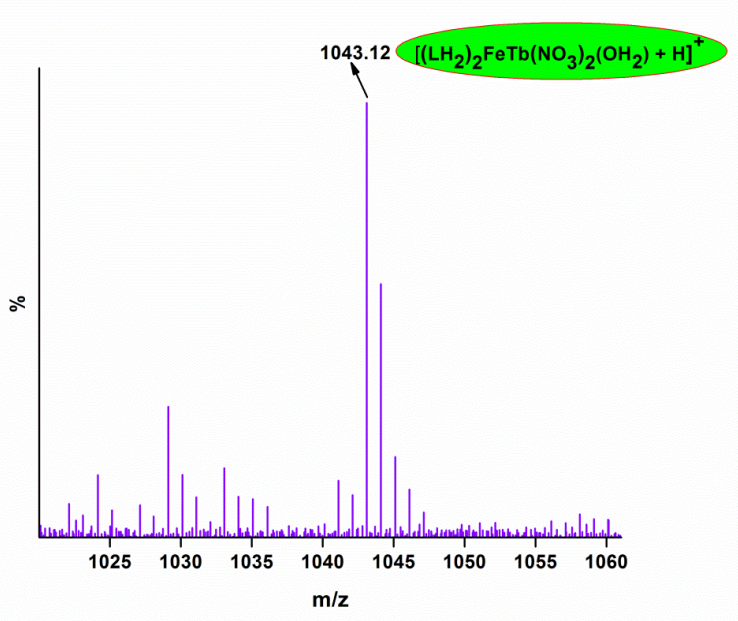

Figure S8. ESI-MS of **3** (shows isotropic distribution pattern of one fragment).

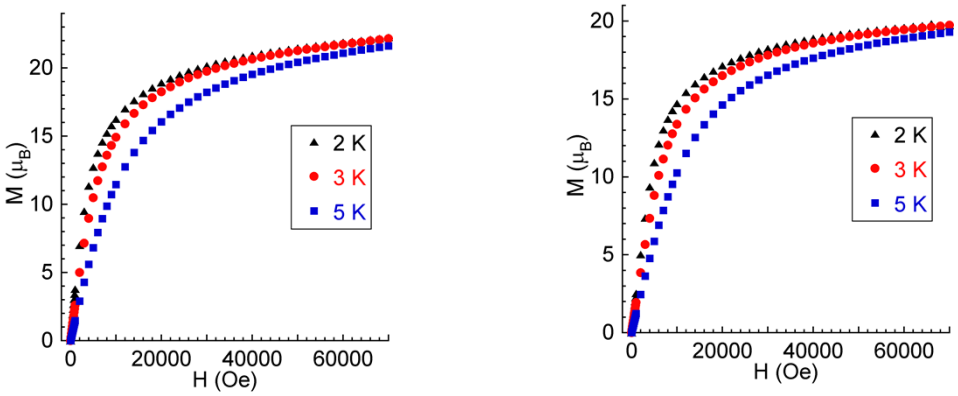

Figure S9. Field dependence of magnetization at low temperatures for **2**(left) and **3**(right)

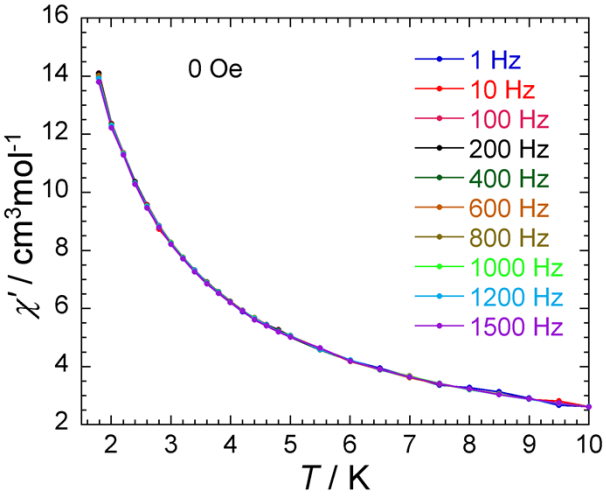

Figure S10. Plot of in-phase *ac* susceptibility signals vs. temperature for **3** (Fe_2Tb_2) at different frequencies, 1-1500 Hz.

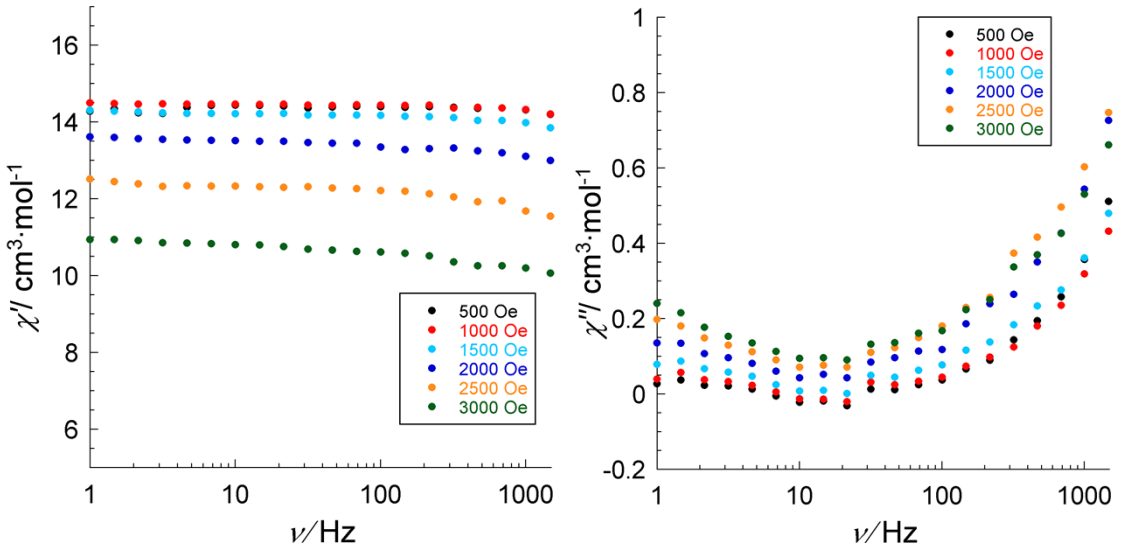

Figure S11. Plots of in-phase (left) and out-of-phase (right) *ac* susceptibility signals vs. frequency for **3** (Fe_2Tb_2) at 1.8 K under the indicated external *dc* fields.

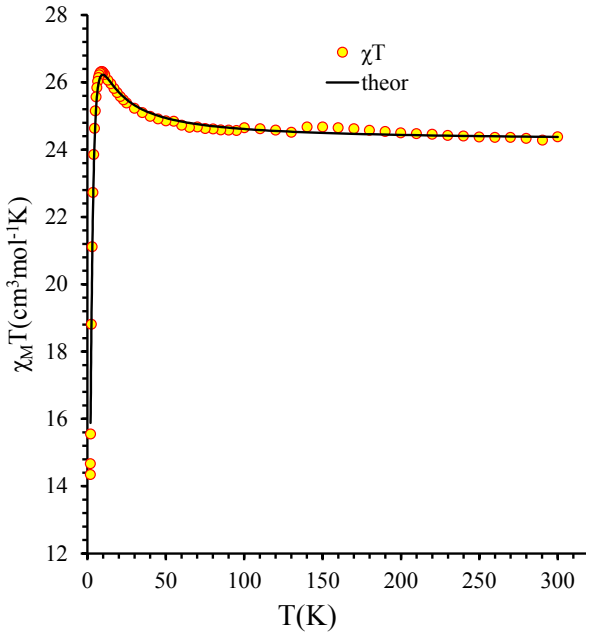

Figure S12. $\chi_M T$ versus T plots data for **1** [Fe_2Gd_2]. The black solid line corresponds to the simulation according the Hamiltonian (1) with parameters described in the text.

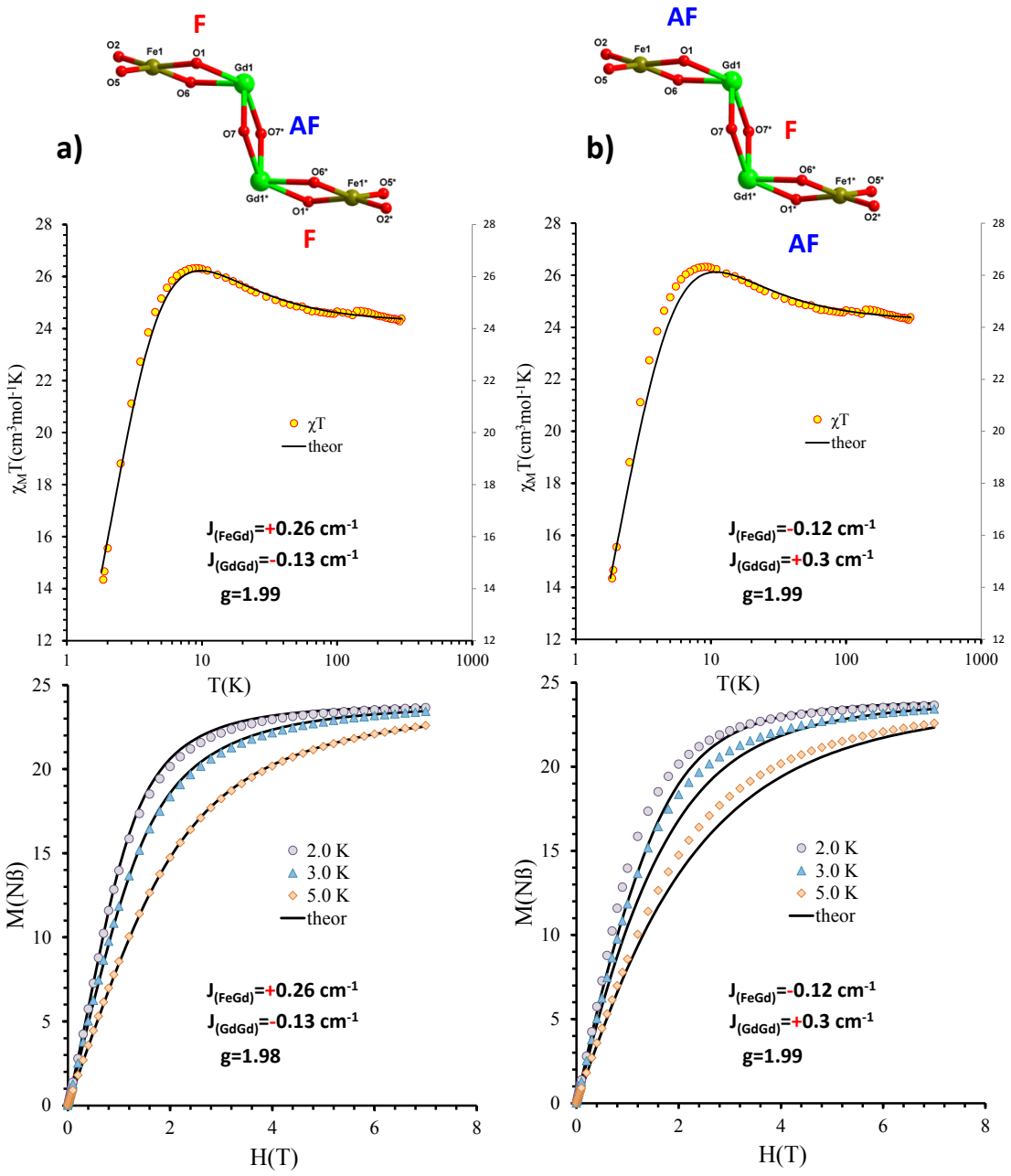

Figure S13. $\chi_M T$ vs.T plots data for **1** [$Fe^{III}_2Gd_2$] top and magnetization curves for **1** [$Fe^{III}_2Gd_2$] at 2, 3 and 5 K. The black solid lines correspond to the simulation according the Hamiltonian (1) with two sets (a) J(FeGd) ferro J(GdGd) antiferro and (b) J(FeGd)antiferro J(GdGd)ferro of parameters used.

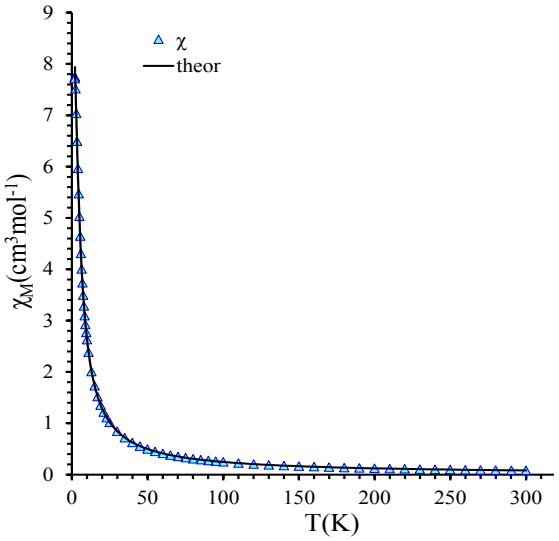

Figure S14. χ_M versus T plots data for **1** [Fe_2Gd_2]. The black solid line corresponds to the simulation according the Hamiltonian (1) with parameters described in the text.

Table S5. Mössbauer data at 50, 3 K in zero-field and at 3 K in applied magnetic field.

Compound, temperature, applied field	δ[a], mm/s	ΔE_Q or ε[c], mm/s	Γ, mm/s	θ, ^{o}	B_{eff}, T
Fe_2Gd_2, **(1)** 50K	0.46(1)	0.30(1)	0.33(2)	-	-
Fe_2Dy_2, **(2)** 50K	0.45(1)	0.30(1)	0.30(2)	-	-
Fe_2Dy_2, **(2)** 3K, 3T	0.48(1)	-0.05(1)	0.44(1)	65.1	50.5(7)
Fe_2Tb_2, **(3)** 50K	0.46(1)	0.31(1)	0.30(1)	-	-
Fe_2Tb_2, **(3)** 3K	0.49(1)	-0.05(1)	0.64(2)	47.0	52.7(4)
Fe_2Tb_2, **(3)** 3K, 3T	0.49[b]	-0.04(1)	0.42(2)	66.2	50.2(1)

[a] Relative to α-Fe at room temperature. [b] Fixed values. [c] For magnetically-split spectra the quadrupole shifts, $\varepsilon = \frac{1}{2}\Delta E_Q(3\cos^2\varphi-1)$. φ - Euler angle between the B_{int} and the main electrical field gradient (EFG) principal axis (V_{zz}). δ is the isomer shift, ΔE_Q - quadrupolar splitting, θ - angle between B_{eff} and direction of γ-rays. The statistical errors are given in parentheses.

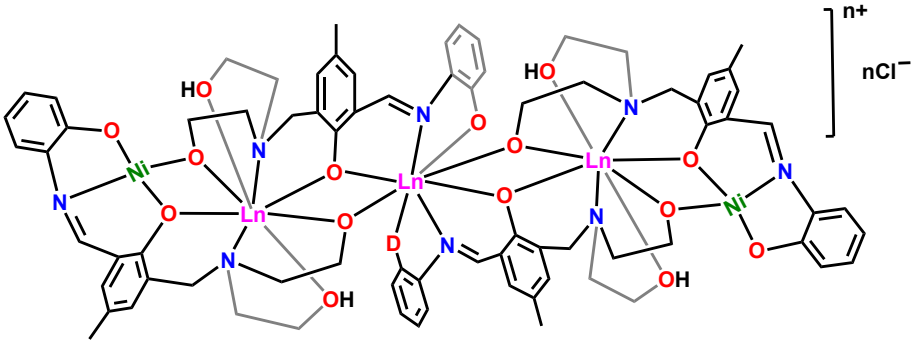

Ln = Gd, Dy, Tb, Ho

D = O (**Gd, Dy**); OH (**Tb, Ho**)

n = 1 (**Gd, Dy**); 2 (**Tb, Ho**)

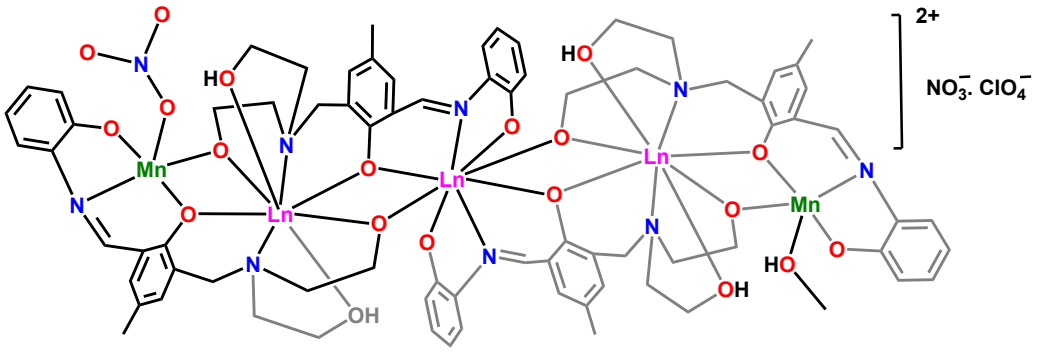

Ln = Gd, Tb, Dy, Ho

Figure S15. Molecular structures of $Ni^{II}_2Ln_3$ (above) and $Mn^{III}_2Ln_3$ (below) series of compounds.

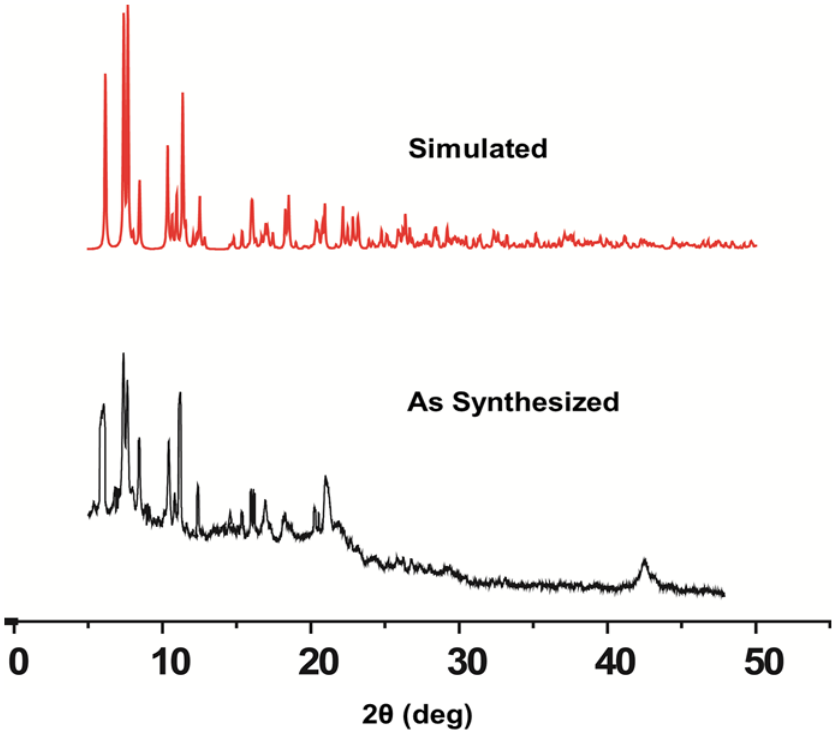

Figure S16. Room temperature PXRD of compound **1** (Fe_2Gd_2).

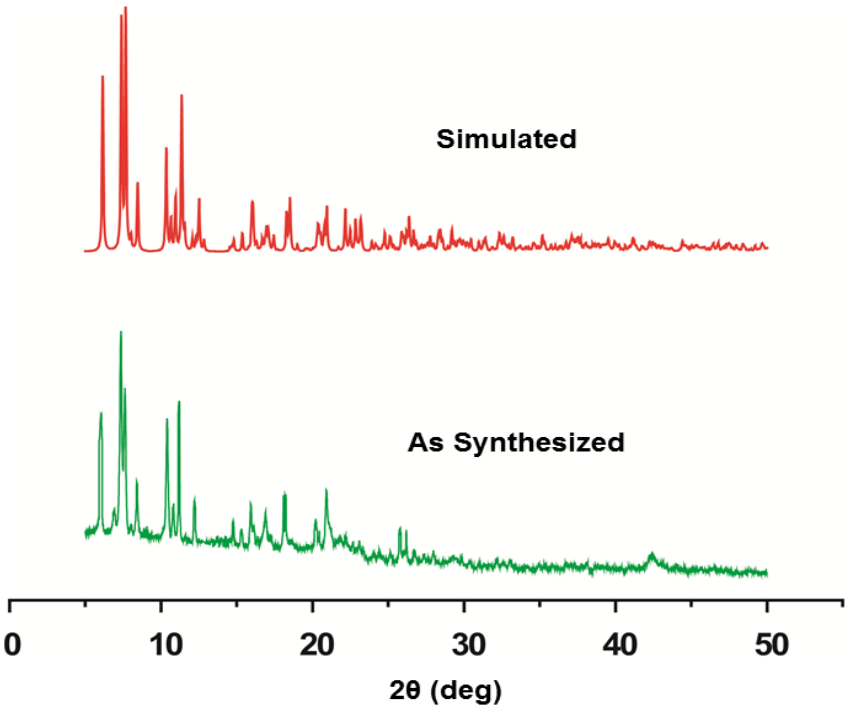

Figure S17. Room temperature PXRD of compound **2** (Fe_2Dy_2).

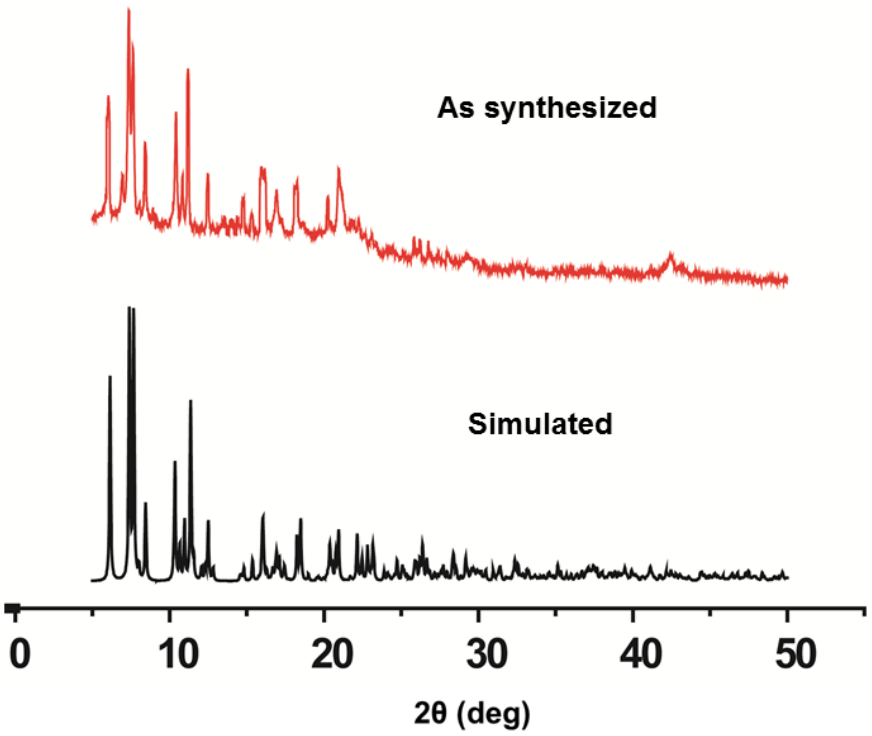

Figure S18. Room temperature PXRD of compound **3** (Fe_2Tb_2).

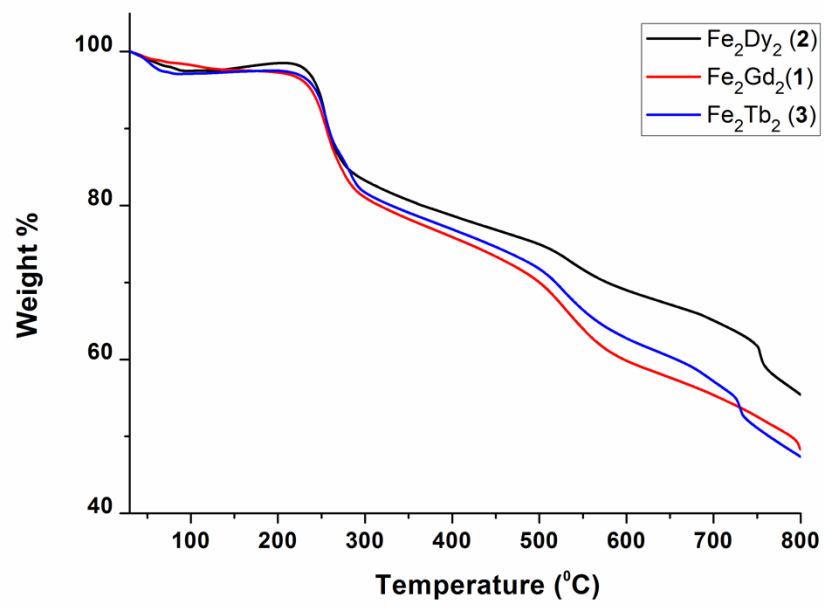

Figure S19. Thermo gravimetric analysis curve of **1, 2** and **3** (Heating rate: 10 °C per min) under argon atmosphere.